DEVELOPMENT OF A GUAR/GELATIN MATRIX CONTAINING LIGNIN DERIVATIVES AND *VACCINIUM VITIS-IDAEA* EXTRACT FOR COSMETICAL USE

IRINA APOSTOL, NARCIS ANGHEL, NATALIA SIMIONESCU and IULIANA SPIRIDON

"Petru Poni" Institute of Macromolecular Chemistry, Grigore Ghica Voda Alley No. 41A, 700487 Iasi, 40 Romania

■ Corresponding author: N. Anghel, anghel.narcis@icmpp.ro

In memory of Acad. Bogdan C. Simionescu

This study developed guar gum-gelatin matrices incorporating Lignoboost lignin, lignin esterified with aspartic acid, lignin esterified with succinic acid, and *Vaccinium vitis-idaea* (Vv) extract for potential skincare applications. Fourier-transform infrared spectroscopy, ¹³C nuclear magnetic resonance spectroscopy, and X-ray photoelectron spectroscopy confirmed successful lignin esterification. Mechanical testing showed that lignin derivatives increased elongation at break (up to 28.15 mm for lignin-containing films), while generally reducing tensile strength compared to the plain matrix (2.79 MPa). The addition of Vv extract reduced flexibility, with lignin succinate-Vv showing the lowest elongation (12.80 mm) and tensile strength (0.37 MPa). The release of lingonberry extract followed the Weibull model (R² values between 0.976–0.996), with diffusion-controlled kinetics. Lignin succinate-Vv achieved the highest release (30.30 mg/g), while lignin-Vv enabled prolonged delivery (~42% release). Anti-inflammatory activity exceeded 58% inhibition of albumin denaturation for lignin succinate-Vv films, and all formulations maintained over 94% fibroblast viability.

Keywords: lignin, skincare product, natural extract release, anti-inflammatory activity

INTRODUCTION

The development of natural and sustainable materials for skincare applications has gained increasing attention in recent years due to the growing demand for eco-friendly products and the need to reduce synthetic additives in skincare formulations. In this context, polymeric matrices consisting of biopolymers, such as guar gum and gelatin, have proven to be promising due to their biodegradability, non-toxicity, and excellent filmforming properties. These natural polymers provide a versatile platform for the incorporation of bioactive compounds, enhancing the biological and mechanical properties of materials.

Guar gum, a polysaccharide extracted from the seeds of *Cyamopsis tetragonoloba*, is widely recognized for its thickening, stabilizing, and emulsifying properties in cosmetic formulations. It forms stable gels and films, making it an excellent choice for structuring cosmetic materials.² Additionally, the high molecular

weight and hydrophilic nature of guar gum enable it to maintain high moisture levels on the skin, contributing to hydration and protection.³

Gelatin, a protein derived from the partial hydrolysis of collagen, is another valuable component used in topical applications. It possesses excellent film-forming capabilities and biocompatibility. Its antigenic activity is proper for biomedical applications, particularly in wound healing, where it aids hemostasis and supports cell adhesion and proliferation.⁴ Gelatin-based films are known for their ability to adhere to the skin, providing a protective barrier and promoting active ingredient delivery. However, gelatin applications are limited because of the poor mechanical properties and low thermal stability, which can be improved through cross-linking or blending with other polymers.⁵ To further enhance the functional properties of guar and gelatin-based materials, bioactive fillers, such as

Cellulose Chem. Technol., **59** (7-8), 875-892(2025)

lignin, lignin aspartate, lignin stearate, and Vaccinium vitis-idaea (lingonberry) extract have been incorporated into the matrix. Lignin, a complex aromatic biopolymer⁶ derived from plant cell walls, offers antioxidant, UV-protective, and antimicrobial properties, making it a valuable component for skincare formulations. However, the hydrophobic nature of lignin can limit its dispersion in hydrophilic matrices.⁷ To address this challenge, esterification with aspartic and succinic acids have been employed to enhance both compatibility with the polymeric matrix, as well as its bioavailability. Lignin aspartate and lignin succinate offer unique advantages due to their modified surface characteristics. Lignin aspartate presents polar functional groups that improve hydrophilicity. Moreover, being an amino acid naturally found in the body, aspartic acid improves the biocompatibility of the material.8 Succinic acid introduces carboxyl (-COOH) functional groups into the lignin structure, providing enhanced lipophilic properties and skin adherence.^{9,10} These modified lignins not only serve as structural fillers, but also contribute to the antioxidant and protective properties of the materials.

Lingonberry extract is rich in flavonoids, anthocyanins, and other phenolic compounds, which are well known for their potent antioxidant and anti-inflammatory properties. These bioactive compounds protect the skin from oxidative stress and reduce inflammation.¹¹ It is expected that the incorporation of *Vaccinium vitis-idaea* extract will enhance the bioactivity of the composite materials.

The synergistic combination of polysaccharides, proteins, and antioxidant compounds yields multifunctional materials with promising applications in skincare, including facial masks, wound dressings, and protective films. By integrating natural polymers with bioactive fillers, these formulations not only meet the growing demand for sustainable and biocompatible solutions, but also enhance the functional performance and therapeutic efficacy of the final products.¹²

Achieving a balance between mechanical strength and bioactivity is crucial for the practical use of thin films. The addition of lignin and its derivatives not only enhances the tensile strength, elasticity, and thermal stability of the films, but also ensures their durability in real-world applications. The bioactive properties imparted by *Vaccinium vitis-idaea* extract further expand their

utility, offering a comprehensive approach to designing advanced functional materials.

This study aims to investigate the obtaining, characterization, and cosmetic potential of guar/gelatin-based materials containing lignin, lignin aspartate, lignin stearate, and Vaccinium vitis-idaea extract. The influence of added compounds on the structural, mechanical, and biological properties of the materials evaluated to understand their suitability for cosmetic applications. The findings contribute to the development of innovative and sustainable materials for the cosmetic industry, aligning with growing demand for natural environmentally friendly products.

EXPERIMENTAL

Materials and methods

Guar gum (Gu), gelatin (Ge), methanol, dimethyl sulfoxide (DMSO), aspartic acid, succinic acid, lipase, ethyl ether, aluminum chloride (AlCl₃), sodium chloride (NaCl), monopotassium phosphate (KH₂PO₄), disodium phosphate (Na₂PO₄·12 H₂O), sodium carbonate (Na₂CO₃) and sodium acetate (CH₃COONa) were all purchased from Sigma-Aldrich (USA). Softwood lignin (Lignoboost softwood - LB) was obtained at Södra Cell, Sweden, by a regular Lignoboost process. Folin-Ciocalteu reagent, 2,2diphenyl-1-picrylhydrazyl (DPPH), gallic acid and quercetin were acquired from FlukaTM (USA), while ethanol and acetic acid were purchased from Chimreactiv SRL. Vaccinium vitis-idaea fruits were extracted with ethanol-water (60:40, v/v) solution for 20 min at 55 °C. 13 The solution was evaporated to dryness using a rotary evaporator under vacuum conditions and the obtained Vv extract was used as filler.

Esterification reaction of lignin

LB was esterified with aspartic and succinic acid, according to the method presented in a previously published paper. Lignin (1 g) and the aspartic or succinic acid (1 g) were solubilized in DMSO. Then, lipase (0.2 g), which acts as catalyst, was added. The reaction mixture was gently stirred at room temperature for 72 h. The solvent was then evaporated at 70 °C under a pressure of 40 mbar. The resulting compounds were washed several times with ethyl ether and water. The obtained lignin esters (LBAs – lignin aspartate and LBSc – lignin succinate) were dried at 60 °C and ground into a fine dark-brown powder.

Preparation of thin films

Solutions of Gu and Ge were prepared and mixed until complete homogenization. Then, Vv extract, LB, LBAs and LBSc were added into the prepared polymeric matrix solution (Table 1) and mixed at room

temperature for 1 h to ensure their complete dispersion. Each mixture was poured into Petri dishes, and the materials were obtained by the casting method.

Total phenolic content (TPC) and total flavonoids content (TFC) in *Vaccinium vitis-idaea* extract

The total phenolic content (TPC) of the *Vaccinium vitis-idaea* extract (Vv) was evaluated using the Folin–Ciocalteu colorimetric method, as previously described by Aryal *et al.*,¹⁵ with minor modifications. 0.5 mL of the extract solution (1 mg/mL) was mixed with 2 mL of a 1:10 (v/v) diluted Folin–Ciocalteu reagent. After a 3-minute reaction time at room temperature, 4 mL of 7.5% (w/v) sodium carbonate (Na₂CO₃) solution was added. The reaction mixture was then incubated in the dark at ambient temperature for 60 minutes to allow chromophore development. Absorbance was recorded at 760 nm using a UV–Vis spectrophotometer (Jenway

6405), with deionized water as blank. Gallic acid was used as the standard for the calibration curve, prepared in concentrations ranging from 0.0024 to 0.156 mg/mL. The TPC in the extract was expressed as gallic acid equivalents (GAE) (mg GAE/g extract).

The total flavonoid content (TFC) of the *Vaccinium vitis-idaea* extract (Vv) was assessed using the aluminum chloride (AlCl₃) colorimetric assay, ¹⁶ with slight procedural adjustments. 2 mL of the extract solution (1 mg/mL) was mixed with 2 mL of 2% (w/v) AlCl₃ prepared in methanol. The reaction mixture was kept in the dark at room temperature for 40 minutes to facilitate the formation of a stable yellow complex. Absorbance was measured at 430 nm using a UV–Vis spectrophotometer. Methanol was used as the blank, and a standard curve was prepared using quercetin (0.5–100 mg/L) and the TFC was expressed as quercetin equivalents (QE) (mg QE/g extract).

Table 1
Material composition (100 mL of solution; polysaccharide matrix: guar – 0.7 g; gelatin – 0.7 g)

Material	Lignin or lignin ester	Vaccinium vitis-idaea extract
Gu/Ge	_	_
Gu/Ge/LB	0.1 g	_
Gu/Ge/Vv	_	0.1 g
Gu/Ge/LB/Vv	0.1 g	0.1 g
Gu/Ge/LBAs	0.1 g	-
Gu/Ge/LBAs/Vv	0.1 g	0.1 g
Gu/Ge/LBSc	0.1 g	-
Gu/Ge/LBSc/Vv	0.1 g	0.1 g

Fourier transform infrared spectroscopy (FTIR)

A Vertex 70 FTIR spectrometer from Brüker, equipped with an ATR (Attenuated Total Reflectance) device (ZnSe crystal) was used to recorder the FTIR spectra of the obtained materials. Those were analyzed in the range of 4000–600 cm⁻¹, with an average of 64 scans and a spectral resolution of 2 cm⁻¹, at a 45 angle of incidence.

¹³C nuclear magnetic resonance (¹³C NMR) of lignin

The solid-state ¹³C NMR spectra were recorded on a Bruker AvanceHD-400 MHz NMR spectrometer operating at a ¹³C resonance frequency of 106 MHz, equipped with a commercial Bruker double-channel probe. Approximately 10–20 mg of the samples was placed in 3.2-mm outer diameter zirconium dioxide rotors and spun at a Magic Angle Spinning (MAS) rate of 15 kHz. The CP technique was employed with a ramped 1H-pulse, starting at 100% power and decreasing to 50% during the contact time (2.5 ms) to avoid Hartmann-Hahn mismatches. A dipolar decoupling GT8 pulse sequence was applied during the acquisition time to enhance resolution. For improved signal-to-noise ratio in the ¹³C CPMAS experiment, 30 K scans were accumulated with a 2.5 s delay. The ¹³C

chemical shifts were referenced to tetramethylsilane and calibrated using the adamantane –CH signal, set at 38.48 ppm.

X-ray photoelectron spectroscopy (XPS) of lignin esters

XPS was performed on an Axis Nova device (Kratos Analytical, Manchester, United Kingdom), using AlK α radiation with 20 mA current and 15 kV voltage (300W), and a base pressure of $10^{-8} \div 10^{-9}$ Torr in the sample chamber. The incident monochromated X-ray beam was focused on a 0.7 mm x 0.3 mm area of the surface. The XPS survey spectra for the samples were collected in the range of $-5 \div 1200$ eV with a resolution of 1 eV and a pass energy of 160 eV. The high-resolution spectra for all the elements identified from the survey spectra were collected using a pass energy of 20 eV and a step size of 0.1 eV. The acquisition of all spectra and survey spectra processing was performed using ESCApe software.

Weight loss (in vitro biodegradability)

The *in vitro* biodegradability of the materials was evaluated by immersing them in a PBS solution (pH = 7.4). Their initial weight was measured and then they were immersed in 10 mL of PBS solution at 37 °C.

After 24 hours, the samples were withdrawn, thoroughly dried at room temperature for 24 hours, and weighed again. The degradation rate was calculated using Equation 1:

Weight loss (%) =
$$\frac{w_i - w_d}{w_i} \times 100$$
 (1) where w_i and w_d are the initial and dried weight of the

samples, respectively.

Porosity

The samples were cut into the desired shape, weighed and immersed into ethanol. After 1 h, the samples were carefully withdrawn from the solution and weighed again. The materials' porosity was

calculated using the following equation (Eq. 2):
Porosity (%) =
$$(\frac{W_w - W_d}{d \times V}) \times 100$$
 (2)

where W_w represents the weight of the wet material, W_d is the weight of the dry material, d represents the density of ethanol (0.78 g/cm 3) while V is the material volume.

Moisture adsorption capacity

The moisture adsorption capacity of the studied materials was examined as described by Madihalli et al. 17 Film samples were cut, weighed to determine the initial weight (w_i) and heated at 100 °C for 24 h. Then, the samples were exposed to room conditions (23 °C, and 50% relative humidity) for 24 h. After that, the samples were re-weighed to determine their final weight (w_f) . The moisture adsorption capacity was calculated using Equation 3:

Moisture adsorption capacity (%) =
$$\frac{w_f - w_i}{w_i} \times 100$$
 (3)

Opacity

The UV-Vis absorption spectra of the materials were recorded using the UV-Vis spectrophotometer. Samples measuring 3×1 cm were placed in quartz cuvettes, and spectra were acquired, with air serving as the reference baseline. Each measurement was performed in triplicate, and the average values were reported. Film opacity was evaluated at 315, 400 and 600 nm, calculated according to Equation 4, where absorbance was normalized by the film thickness, x (mm):¹⁷

Opacity =
$$\frac{Absorbance}{x}$$
 (4)

Density

The compactness and structural integration of fillers within the polysaccharide matrix were evaluated through density measurements. Material density was determined using the pycnometer method,18 in which the volume of the solid sample was indirectly obtained from the displacement of ethanol. The density was

calculated according to Equation 5:

$$d_{s} (g/cm^{3}) = \frac{m_{s}}{v_{s}} = \frac{m_{s}}{(m_{a} + m_{s} - m_{as}) \times d_{a}}$$
(5)

where m_s is the weight of the studied material, v_s represents the volume of the studied material, m_a

represents the weight of the pycnometer completely filled with ethanol, m_{as} is the weight of the pycnometer, which contained the studied materials (the remaining free volume of the pycnometer was filled with ethanol), and $d_{ethanol}$ represents the ethanol density (0.789 g/cm³).

Swelling index

To evaluate the swelling index, each material was cut into the desired shape. The initial weight of each fragment was measured (w_d) . The fragments were then added to solutions of pH 4, 5.5 and 7 at room temperature. The pH values were adjusted using CH₃COONa and CH₃COOH. After 1 h, the samples reached the equilibrium state and were taken out of the flask, and excess water was removed. The hydrated films were weighed (w_s) and their swelling index¹⁹ was calculated using Equation 6:

Swelling index (%) =
$$\frac{w_s - w_d}{w_d} \times 100$$
 (6)

Tensile properties

Mechanical tests took place at 50% relative humidity and 23 °C. Young's modulus (MPa), breaking tensile stress (MPa) and elongation at break (mm) were determined using an Instron 1000 N test machine (Norwood, MA, USA) operated at a test speed of 10 mm/min.

Scanning electron microscopy (SEM)

Scanning electron microscopy (SEM) employed to investigate the surface morphology and microstructural homogeneity of the films, providing an insight into filler distribution and matrix-filler interfacial compatibility. SEM images were acquired using a VEGA TESCAN microscope equipped with a low-vacuum secondary electron detector, operated at an accelerating voltage of 20 kV under ambient temperature conditions.

In vitro Vv extract release study

The in vitro release study was performed to investigate the release behavior of the Vv extract. The materials (0.1 g) were introduced in 25 mL of distilled water, at room temperature. At different time intervals, the solutions were analyzed using the UV-Vis spectrophotometer, at 325 nm. The concentration of the Vv extract was determined by using a calibration

A critical phase in the development of controlled delivery systems involves understanding the kinetic the properties governing release processes. Mathematical modelling serves as a powerful tool enabling researchers to characterize, compare, and various formulations under optimize distinct experimental conditions. Widely utilized kinetic models in pharmaceutical and nutraceutical research include the Higuchi, Korsmeyer-Peppas, Hixson-Crowell, Gompertz, and Makoid-Banakar models, each offering distinct perspectives on the underlying

mechanisms of release, such as diffusion-controlled, erosion-controlled, or complex combinations involving swelling and polymer relaxation.¹⁸

The Higuchi model (Eq. 7) specifically addresses diffusion-controlled release from solid matrices, based on Fick's law of diffusion, assuming a pseudo-steady-state condition with drug concentrations within the matrix remaining above their solubility limits. The cumulative release (M_t) at time (t) is expressed by:

$$M_t = k_H \times t^{1/2}$$
 (7)

where k_H represents the Higuchi rate constant. This model accurately characterizes drug release in topical formulations, polymeric matrices, and transdermal systems predominantly driven by diffusion.

The Korsmeyer-Peppas model (Eq. 8) provides an empirical framework suitable for analyzing drug release from polymeric systems exhibiting multiple simultaneous mechanisms, such as diffusion, swelling, and erosion. The mathematical relationship is:

$$M_t/M_{\infty} = k \times t^n \tag{8}$$

where k denotes the release rate constant and n indicates the release exponent. This exponent helps discern the mechanism: $n \leq 0.5$ signifies Fickian diffusion, values between 0.5 and 1 indicate anomalous (non-Fickian) transport due to combined diffusion and polymer relaxation, and $n \geq 1$ signifies erosion-dominated release. The Korsmeyer-Peppas model is extensively applied to hydrogels, biodegradable polymers, and nanoparticle-based delivery systems.

The Hixson-Crowell cube root law (Eq. 9) is designed to describe systems experiencing a progressive reduction in surface area during drug release, such as dissolving tablets or eroding particles. The fundamental assumption is that the rate of release directly correlates with the available surface area for dissolution, given by:

dissolution, given by:

$$M_0^{1/3} - M_t^{1/3} = k_{HC} \times t$$
(9)

where M_0 and M_t represent the initial and remaining drug mass at time t, respectively, and k_{HC} is the dissolution rate constant. This model is primarily suitable for oral dosage forms like tablets and granules, where erosion significantly influences drug release.

The Gompertz model (Eq. 10) is suitable for drug release profiles displaying a sigmoidal shape, characterized by an initial acceleration in release rate followed by a deceleration over time. This model effectively describes scenarios driven by polymer degradation, enzyme-mediated processes, or swelling-controlled mechanisms, and is mathematically represented by:

$$M_t = M_{\infty} \times e^{-\beta e^{-\alpha t}} \tag{10}$$

where α is the release rate constant (controlling system responsiveness) and β is the lag factor (initial resistance to drug release). The Gompertz model has been effectively applied to nanoparticles, liposomes, and biodegradable polymers exhibiting an initial resistance, subsequent rapid release, and eventual saturation.

The Makoid-Banakar model (Eq. 11) is an empirical equation designed for complex controlled-release behaviors, especially those involving an initial lag phase followed by exponential release dynamics. The model is represented as:

$$M_t = M_{\infty} \times \left(1 - e^{-kt^n}\right) \tag{11}$$

where M_{∞} is the equilibrium drug release, k is the rate constant, and n is an exponent capturing variation in release behavior. This model has proven valuable in characterizing polymeric delivery systems, such as microspheres and hydrogels, where the interplay of diffusion and polymer relaxation significantly affects drug release.

Anti-inflammatory activity of the materials

The anti-inflammatory activity of the materials was investigated using the egg albumin denaturation method, as described by Ameena et al.,20 with a few modifications. Initially, a stock solution was prepared by mixing 40 mL of fresh egg albumin with 140 mL of phosphate-buffered saline solution (PBS, pH 6.4, 10 mM). The resulted mixture was then filtered to remove any particulate matter. From the filtered solution, 2 mL was taken and diluted with an additional 2 mL of PBS, followed by incubation at 35 °C for 30 minutes and heating at 70 °C for 5 minutes to induce denaturation. The appearance of opalescence was monitored as an indicator of protein denaturation. The absorbance of the solution was measured at 660 nm using the UV-Vis spectrophotometer, after cooling. This represented the control sample for further comparisons.

The same procedure was applied to the analyzed materials, with the addition of 0.02 g of each sample to the prepared egg albumin solution. After incubation at 35 °C for 10 minutes, the solutions were filtered to remove any insoluble residues. The filtered solutions were then heated at 70 °C for 10 minutes to induce denaturation. The degree of inhibition of protein denaturation was calculated using Equation 12:

This calculation allowed the determination of the percentage inhibition of denaturation for each sample.

Antioxidant activity of the materials

To evaluate the antioxidant capacity of the obtained materials, the method used by Altinkaynak *et al.*,²¹ with a few modifications, was used. 0.0265 g of sample was added to 3 mL of ethanol. Then, 1 mL of 0.1 mM DPPH solution (prepared in ethanol) was added. The reaction solutions were incubated in a dark place at room temperature. After 30 minutes, the absorbance of the solutions was measured at 517 nm using the spectrophotometer. The blank solution was ethanol. The DPPH free radical scavenging activity was determined using Equation 13:

DPPH radical scavenging activity (%) =
$$(1 - \frac{Absorbance\ of\ sample}{Absorbance\ of\ control}) \times 100$$
 (13)

where *Absorbance of control* is the absorbance of the reaction solution without sample. The experiment was done in triplicate.

In vitro biocompatibility (MTS assay)

Human dermal fibroblasts (HDF, CLS Cell Lines Service GmbH, Eppelheim, Germany) were seeded (5 × 10⁴ cells/mL) into tissue culture-treated 96-well plates. The biocompatibility of the samples was assessed with the MTS assay, using the CellTiter 96® AQueous One Solution Cell Proliferation Assay (Promega, Madison, WI USA), according to the manufacturer's instructions. Samples (10 mg/mL) were extracted over 24 h, at 37 °C, in complete cell culture medium: MEMα medium with 10% fetal bovine serum 1% Penicillin-Streptomycin-Amphotericin B mixture (all from PAN-Biotech GmbH, Aidenbach, Germany). Active compounds were tested at concentrations equivalent to those found in the samples. Cells were incubated with fresh complete medium (control) or diluted samples' extracts (0.25/0.5/0.75/1 mg/mL) for 24 h. MTS absorbance at 490 nm was recorded on a FLUOstar® Omega microplate reader (BMG LABTECH, Ortenberg, Germany). Experiments were done in triplicate and cell viability in the presence of the sample extracts was expressed as percentage of the cell viability in the presence of the control (means \pm standard deviation).

Statistical analysis

All the experimental analyses of the developed materials were conducted considering statistical significance. The data analyzed in this paper were averaged from at least three replicates. The results were presented as mean \pm standard deviation.

RESULTS AND DISCUSSION TPC and TFC of Vv extract

The TPC of the Vv extract was 37.02 mg GAE/g extract and TFC was 84.0 mg QE/g extract. According to Xu *et al.*, these values are characteristic of extracts obtained from fully ripened Vv fruits.²² It is expected that these bioactive compounds will impart anti-inflammatory, antioxidant and therapeutic properties to the materials.

FTIR spectra of Vv extract

FTIR spectra of the Vv fruits extract is presented in Figure 1. The band in the region between 1200–1000 cm⁻¹ is assigned to the stretching vibration of C–OH side groups, and the glycoside bond (C–O–C) vibrations in polysaccharide chains, while the band at 3394 cm⁻¹ is specific to

the stretching vibration of –OH groups. The peak at 2929 cm⁻¹, characteristic of the asymmetric stretching vibration of –CH₂ is also present. The bands in the range of 933–808 cm⁻¹ are due to the oscillation of the anomeric region of carbohydrates, α/β –glycosidic linkage or C–H deformation. Specific vibrations in the region of 1514–1423 cm⁻¹ are attributed to phenolic fragments and phenyl hydroxyl structure.²³

FTIR spectra of LB and LB esters

In Figure 2, the FTIR spectra of LB and its esters are presented. The FTIR profile of the native lignin (LB) displays the expected broad O-H stretching envelope centered around 3400 cm⁻¹, together with aliphatic C-H stretches at ca. 2930-2845 cm⁻¹. The aromatic framework is evident from the ring skeletal bands at ~1600 and ~1510 cm⁻¹, CH deformation near 1460 cm⁻¹, and the guaiacyl/syringyl-associated C-O vibrations between ~1260 and ~1030 cm⁻¹, with out-of-plane aromatic C-H below 900 cm^{-1} . esterification, both modified samples exhibit a pronounced new carbonyl band in the 1720-1735 cm⁻¹ region, characteristic of ester C=O and markedly more intense than in LB, confirming successful acylation of lignin hydroxyls.²⁴ Concomitantly, the O-H envelope narrows and decreases intensity, consistent in consumption of phenolic/aliphatic OH groups during ester formation.

The lignin-aspartic acid ester (LBAs) retains the aromatic bands, but shows additional nitrogen-containing features absent from LB and LBSc: a weak N-H stretching component overlapping the high-wavenumber region and amide/amine fingerprints manifested as bands around $\sim 1650-1630$ cm⁻¹ (amide I/ δ N–H/C=O contributions) and $\sim 1540-1530$ cm⁻¹ (amide II/δN–H coupled with C–N stretching). A C– N/C-O-C complex vibration is also reinforced in cm⁻¹ window, 1280-1220 supporting incorporation of the amino acid residue. By contrast, the lignin-succinic acid ester (LBSc) lacks the nitrogen signatures and instead accentuates the ester carbonyl near ~1725 cm⁻¹ together with strong C-O-C stretches at ~1175-1120 cm⁻¹; the aliphatic C–H region often gains intensity owing to the introduced succinyl methylene groups.²⁵ In both esters, the persistence of the ~1600/1510 cm⁻¹ aromatic modes indicates that the lignin backbone remains intact, while systematic changes in the hydroxyl, carbonyl and C-O/N spectral domains substantiate successful

derivatization, amino acid functionalization for LBAs and purely aliphatic diacid esterification for LBSc.

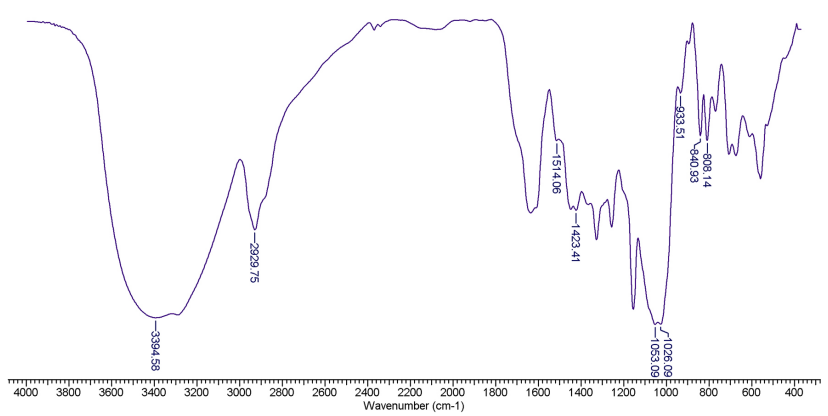


Figure 1: FTIR spectra of the Vv extract

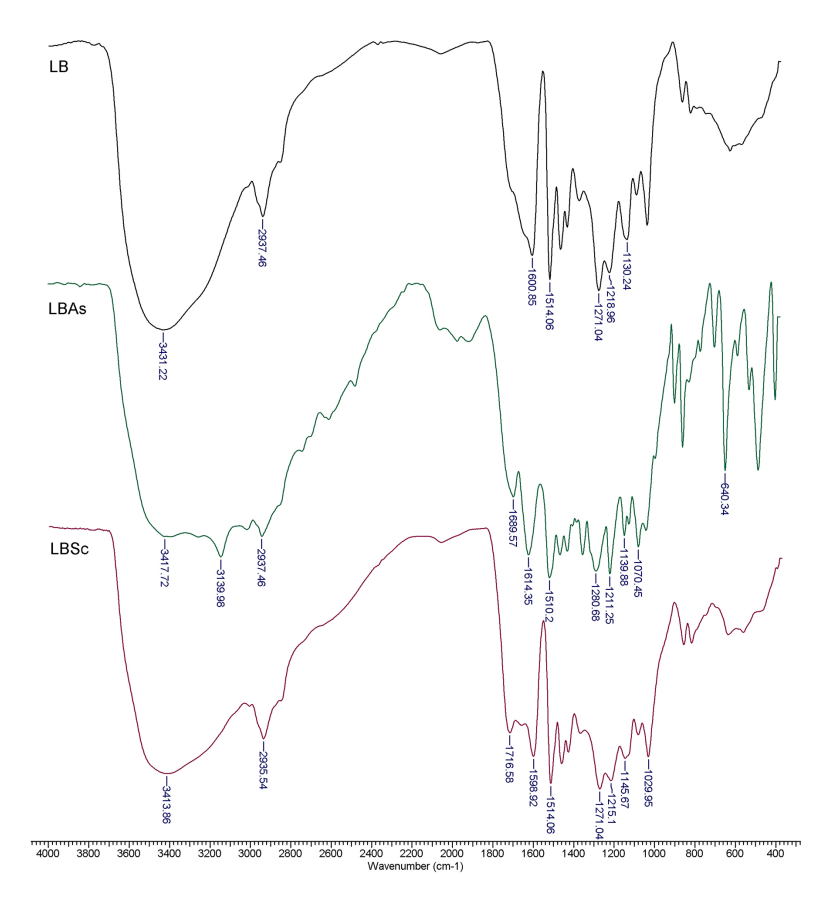


Figure 2: FTIR spectra of LB, LBAs and LBSc

¹³C NMR spectra of LB and LB esters

The ¹³C NMR spectra of LB, LBSc, and LBAs are shown in Figure 3. All samples exhibit characteristic signals of lignin in the aromatic region (δ 150–110 ppm), corresponding to guaiacyl and syringyl units. Esterification induced

noticeable spectral changes, particularly in the carbonyl region (δ 185–160 ppm), where new signals attributable to ester functionalities were observed in both LBSc and LBAs. ²⁶ In the case of LBAs, additional carbonyl resonances consistent with amide groups were detected, confirming the incorporation of aspartic acid moieties.

The aliphatic–oxygenated region (δ 90–60 ppm) displayed variations in peak intensity and pattern upon modification, reflecting the introduction of oxygenated carbons from the esterifying agents. Furthermore, new signals in the aliphatic region (δ 30–20 ppm) in LBSc and LBAs are assigned to methylene groups of the succinic and aspartic acid chains, respectively.

Compared to LBSc, LBAs exhibited a more complex spectral profile, in agreement with the presence of both ester and amide functionalities.

The ¹³C NMR results confirm successful covalent functionalization of lignin with both succinic and aspartic acids, with the latter introducing a higher degree of chemical diversity into the polymer structure.

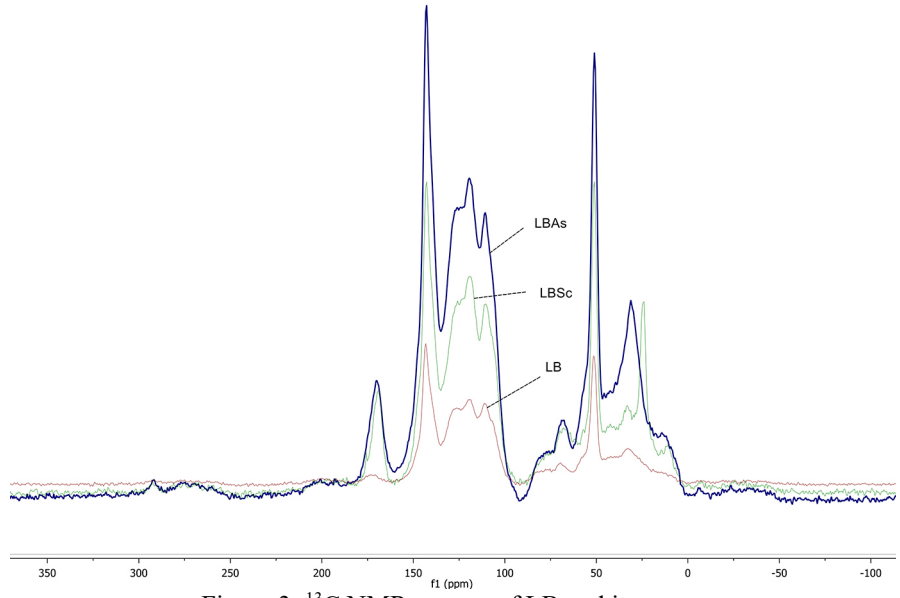


Figure 3: ¹³C NMR spectra of LB and its esters

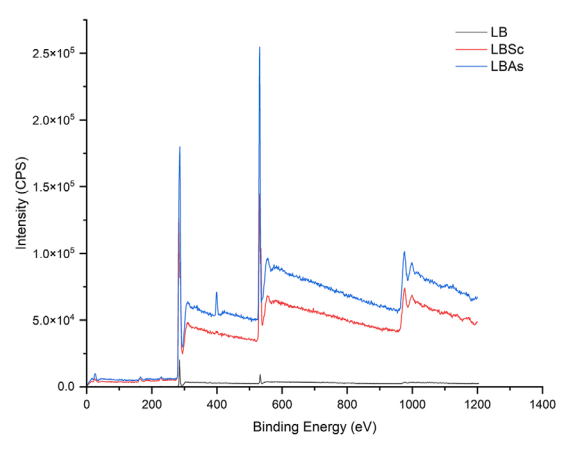


Figure 4: XPS wide scan spectra of LB and its esters

XPS spectra of LB and LB esters

The XPS spectra of unmodified lignin (LB) and the obtained esters (LBSc and LBAs) are presented in Figure 4. All samples exhibited the characteristic C 1s (~284.8 eV) and O 1s (~531–533 eV) signals typical of lignin. In the esterified derivatives (LBSc and LBAs), a marked increase in the relative O 1s intensity was observed, indicative of a higher oxygen content resulting

from the introduction of carboxyl- and estercontaining groups. In addition to the changes in carbon and oxygen signals, the LBAs sample displayed a distinct N 1s peak (~399.5–401.0 eV), which is absent in both LB and LBSc. This nitrogen signal is consistent with amide or amine functionalities derived from the aspartic acid moiety, confirming its covalent incorporation into the lignin structure. Both LBSc and LBAs also exhibited an increase in the high-binding-energy component of C 1s (~288.5–289.0 eV), assigned to carbonyl carbons in ester or amide linkages, and a corresponding increase in the C=O contribution within the O 1s envelope (~531.0–531.6 eV).²⁷

Minor peaks detected in the high binding energy region (~1000–1070 eV) correspond to Na 1s signals, most likely arising from residual inorganic salts introduced during lignin isolation and processing. These features were present in all samples and are not related to the esterification reactions.

Overall, the XPS data confirm the successful functionalization of lignin with succinic and aspartic acids, with LBSc showing chemical signatures consistent with esterification, and LBAs exhibiting additional nitrogen-based functionalities characteristic of amide linkages. The increase in the O/C ratio from LB to LBSc and LBAs, together with the appearance of N 1s

in LBAs, supports the proposed reaction pathways and demonstrates the effectiveness of the modification strategy.

FTIR spectra of biomaterials

FTIR spectra of the obtained materials are presented in Figure 5. Thus, specific peaks of matrix components are present. Signals recorded between 800 and 1200 cm⁻¹ are ascribed to the highly coupled C–C–O, C–OH and C–O–C stretching modes of guar backbone.²⁸ Major peaks in gelatin, such as amide I (1652 cm⁻¹, C=O stretching vibration), amide II (1550 cm⁻¹, N–H bending and C–N stretching) and amide III (1240 cm⁻¹, stretching vibration of C–N and N–H from gelatin) were identified.²⁹ All materials present peaks at 2800–2950 cm⁻¹ corresponding to the aliphatic C–H stretching vibrations from the guar and a broad peak at 3200–3500 cm⁻¹, attributed to O–H and N–H stretching vibrations.

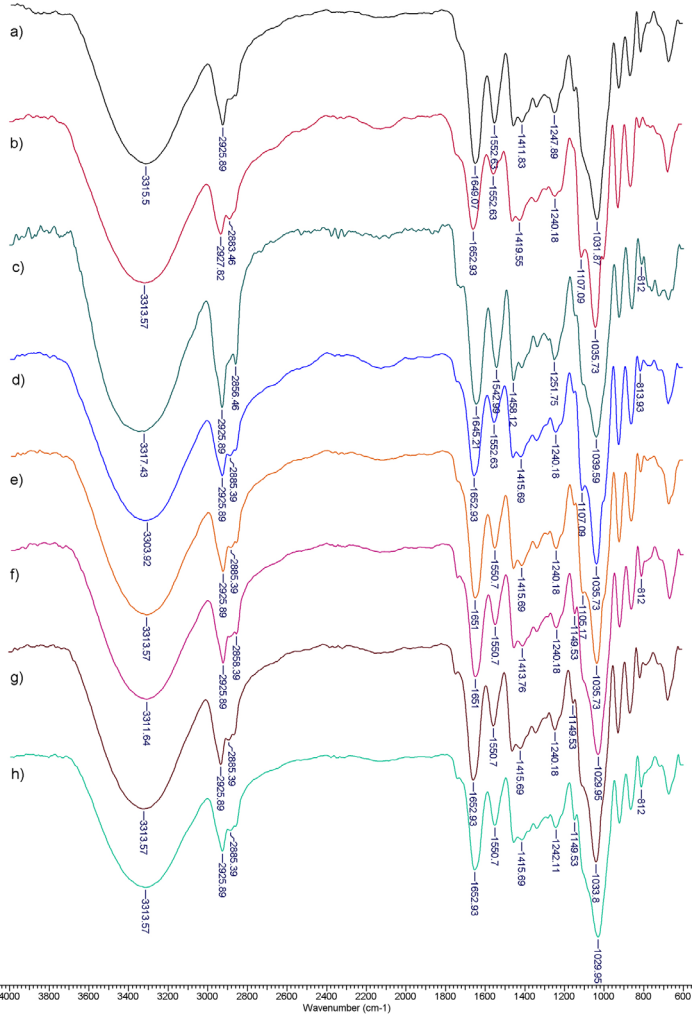


Figure 5: FTIR spectra of Gu/Ge (a), Gu/Ge/LB (b), Gu/Ge/Vv (c), Gu/Ge/LB/Vv (d), Gu/Ge/LBAs (e), Gu/Ge/LBAs/Vv (f), Gu/Ge/LBSc (g), Gu/Ge/LBSc/Vv (h)

Weight loss, porosity and moisture adsorption capacity and density

The correlation between porosity, moisture adsorption capacity, and density in the studied guar-gelatin based composite materials indicates that water retention is influenced by both physical microstructure and chemical composition. In general, higher porosity corresponded to greater moisture adsorption, as the enlarged void network provided a larger accessible surface area for water binding. However, this association was modulated by the hydrophilic-hydrophobic balance of the matrix. For example, Gu/Ge/LBAs/Vv, with the highest porosity (0.0143%), exhibited the greatest moisture adsorption (10.24%), reflecting the contribution of hydrophilic functional groups introduced through lignin-aspartic esterification. In contrast, Gu/Ge/Vv showed relatively higher porosity than Gu/Ge, but significantly lower moisture uptake (5.16%), likely due to the hydrophobic nature of certain phenolic compounds in the Vaccinium vitis-idaea extract that limit water penetration.

The porosity-density relationship followed the expected inverse trend, as greater pore volumes generally reduced the mass per unit volume. Nevertheless, variations in density were not purely structural, but also chemical in origin. The case of Gu/Ge/LBSc/Vv illustrates this: despite having the porosity similar to that of Gu/Ge/LB/Vv, it displayed a markedly higher density (1.939 g/cm³) due to the more compact molecular packing conferred by succinic acid esterification.

The link between moisture adsorption and density proved more complex. While lower density can imply more free volume for water, in these systems, the decisive factor was the surface chemistry and connectivity of pores. Hydrophilic modifications enabled substantial moisture adsorption even in denser structures (e.g., Gu/Ge/LBSc/Vv with 8.22% moisture uptake), while hydrophobic constituents suppressed adsorption despite lower density (e.g., Gu/Ge/Vv).

Table 2
Weight loss, porosity, moisture adsorption capacity and density values of the obtained materials

Material	Weight loss (%)	Porosity (%)	Moisture adsorption capacity (%)	Density (g/cm ³)
Gu/Ge	31.68±0.84	0.00062±0.0003	9.78±0.28	0.753±0.001
Gu/Ge/LB	48.22 ± 1.26	0.00220 ± 0.0019	10.04 ± 0.81	1.070 ± 0.017
Gu/Ge/Vv	21.13 ± 0.85	0.00167 ± 0.0006	5.16 ± 0.71	0.710 ± 0.008
Gu/Ge/LB/Vv	17.38 ± 1.40	0.00884 ± 0.0013	7.26 ± 0.66	1.058 ± 0.015
Gu/Ge/LBAs	28.92 ± 0.73	0.00500 ± 0.0011	5.49 ± 0.74	0.755 ± 0.006
Gu/Ge/LBAs/Vv	30.49 ± 1.69	0.01437 ± 0.0015	10.24 ± 0.56	1.083 ± 0.007
Gu/Ge/LBSc	44.82 ± 0.79	0.00684 ± 0.0017	8.08 ± 0.76	0.939 ± 0.013
Gu/Ge/LBSc/Vv	23.00 ± 1.58	0.00887 ± 0.0010	8.22 ± 0.78	1.939 ± 0.004

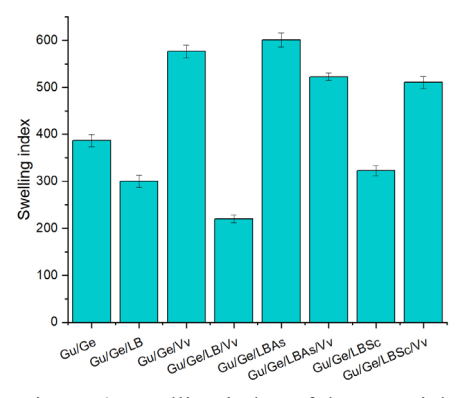


Figure 6: Swelling index of the materials

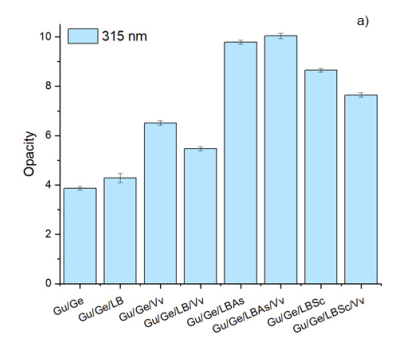
The studied materials exhibit clear compositional effects that override purely physical correlations. Samples containing

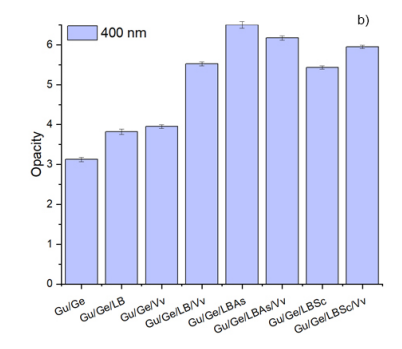
hydrophilic lignin esters (LBAs, LBSc) and higher porosity generally achieved superior moisture adsorption, making them promising candidates for applications requiring water retention. In contrast, the incorporation of Vv extract reduced water affinity, particularly in low-porosity matrices, suggesting potential for moisture-resistant formulations. Thus, tailoring the balance between porosity, density, and surface chemistry enables fine control over sorption behavior in these guar-gelatin based composites.

Swelling index

Swelling index is related to the possible affinity of materials toward water and it is influenced by the available channels for water transmission through the material. A reduction in the availability of hydrophilic hydroxyl groups in the materials as a result of lignin/lignin ester addition led to decreasing the sensitivity of the materials to water. The increment in swelling index (Fig. 6) of the materials comprising lignin/lignin ester and Vv extract might be explained by the hydrogen interactions among hydrophilic functional groups present in Vv phenolic compounds and lignin esters toward water.³⁰

Opacity





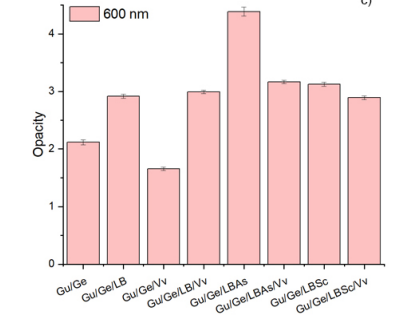


Figure 7: Opacity of the materials

Table 3 Young modulus, elongation at break and tensile strength values of the obtained materials

Sample	Young modulus,	Elongation at	Tensile strength,
Sample	MPa	break, mm	MPa
Gu/Ge	1.05 ± 0.04	22.59±2.11	2.79±1.80
Gu/Ge/LB	1.82 ± 1.02	28.15 ± 2.62	0.89 ± 0.59
Gu/Ge/Vv	0.90 ± 0.04	25.73 ± 1.48	0.39 ± 0.04
Gu/Ge/LB/Vv	2.84 ± 1.02	16.13 ± 1.42	1.72 ± 0.54
Gu/Ge/LBAs	3.57 ± 0.46	24.06 ± 3.94	1.47 ± 0.66
Gu/Ge/LBAs/Vv	4.63 ± 0.30	15.70 ± 1.87	1.22 ± 0.08
Gu/Ge/LBSc	2.21 ± 0.28	23.03 ± 1.86	0.86 ± 0.10
Gu/Ge/LBSc/Vv	1.74 ± 0.17	12.80 ± 3.62	0.37 ± 0.09

The opacity values of the obtained materials varied from 3.86 ± 0.06 to 10.04 ± 0.10 at 315 nm. from 3.12±0.05 to 6.50±0.08 at 400 nm and from 1.66 ± 0.02 to 4.39 ± 0.07 at 600 nm. The lignin and Vv extract markedly increased the materials' opacity, as seen in Figure 7. The augmentation in materials' opacity is attributed to the inherent color and complex structure of lignin and the polyphenols from the extract, which promote light scattering within the polymeric matrix. Also, both lignin/lignin esters, as well as Vv extract could fill the gaps of the polymer matrix, thus the matrix became more compact, impeding the light transmission.³¹ The films comprising LBAs presented the highest opacity at all analyzed wavelengths, proving excellent barrier properties to visible light.

Mechanical properties

Young modulus, elongation at break and tensile strength values of the obtained materials are presented in Table 3. Tensile strength represents the maximum stress the film can sustain before deformation. It varies between 2.79±1.80 (Gu/Ge matrix) and 0.37±0.09 (Gu/Ge/LBSc/Vv) MPa.

This decrement that occurred upon filler addition is caused by the interaction between polymer matrix and fillers, as well as to the partial replacement of polymer-polymer interactions with polymer-fillers contacts, which weakens the film structure, thus reducing the tensile strength.³²The presence of the Vv extract led to a decrease in tensile strength and elongation at break, indicating a more rigid and less flexible structure. The addition of lignin and its derivatives resulted in an increase of elongation at break, while tensile strength showed an opposite trend. It is possible creates a hydrophobic lignin arrangement of the matrix components, a heterogeneous film network and discontinuous microstructure, which influence the mechanical resistance of the materials.³³ The improvement in the elongation at break suggests that lignin/lignin derivatives addition imparts more flexibility to the matrix, which is stretched further before reaching the point of rupture.

Materials morphology

The SEM technique was used to observe the microstructure and dispersion of the added filler into the Gu/Ge matrix. The surface morphology of the materials is shown in Figure 8.

As compared to the smooth surface, without any noticeable defects, of the matrix, the addition of lignin and its esters resulted in holes and cracks, probably because of reduced adhesion between the matrix and the added compounds, which was confirmed by the decrease in mechanical properties. The materials surface became pitted and rough, but no phase separation occurred. Upon the addition of phenolic substances from the Vv extract to the materials comprising lignin/lignin ester, the surface of the composite appeared as only wrinkled, as compared with those containing lignin or lignin ester, which presented some cracked and wrinkled areas.

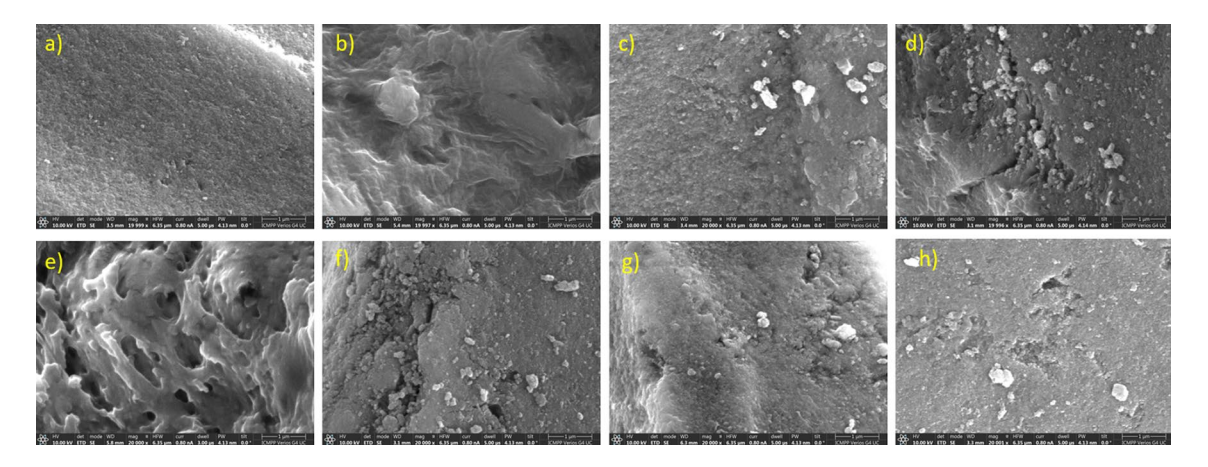


Figure 8: SEM micrographs of Gu/Ge (a), Gu/Ge/LB (b), Gu/Ge/Vv (c), Gu/Ge/LB/Vv (d), Gu/Ge/LBAs (e), Gu/Ge/LBAs/Vv (f), Gu/Ge/LBSc (g), Gu/Ge/LBSc/Vv (h)

Release of Vv extract from the materials

The release kinetics of Vv were systematically analyzed using the aforementioned kinetic models, with the most suitable model determined through statistical parameters and mechanistic rationale. Through comparative modeling, this study aims to identify the predominant release facilitating mechanisms. thereby advancements in optimizing polysaccharide-based controlled delivery systems. The release profiles of the Vv extract from the tested gel-based GuGeLBVv, formulations (GuGeVv, Gu/Ge/LBAs/Vv, and Gu/Ge/LBSc/Vv) are presented in Figure 9 and were further analyzed using various mathematical models. Among these, the Weibull model provided the best fit for the experimental data, as indicated by high determination coefficients ($R^2 > 0.976$ for all formulations) and low reduced chi-squared values (Table 4), suggesting its suitability in describing the release mechanisms involved.

All formulations exhibited a characteristic biphasic release pattern, consisting of an initial rapid release, followed by a slower, sustained phase. The extent and rate of release varied significantly among the formulations. Gu/Ge/LBSc/Vv demonstrated the most pronounced release, reaching a maximum extract

release of approximately 30 mg/g material, with the highest release rate constant (k=0.018) and the lowest shape parameter (d=0.746). These parameters suggest a strong initial burst followed by diffusion-controlled release, likely due to a more porous or hydrophilic matrix facilitating rapid extract diffusion.

Gu/Ge/LBAs/Vv followed with a moderate release profile (A = 19.435 mg/g; k = 0.009), while Gu/Ge/Vv (A = 12.391 mg/g; k = 0.012) and Gu/Ge/LB/Vv (A = 13.076 mg/g; k = 0.005) showed more controlled release behavior. Notably, Gu/Ge/LB/Vv released the smallest amount of extract (~42%) over the monitored period, displaying the slowest kinetics, which is desirable for applications requiring prolonged bioavailability.

The shape factor (d) values for all formulations were less than 1, indicating that Fickian diffusion was the predominant release mechanism across all matrices. These results underline the impact of materials' composition and matrix modification on the release kinetics of phytochemicals.

In summary, the formulation Gu/Ge/LBSc/Vv is most suited for applications demanding rapid and high-yield extract delivery (~98%), while Gu/Ge/LB/Vv appears promising for sustained-

release systems. These findings provide a basis for the tailored design of plant extract delivery platforms based on specific therapeutic needs.

To assess the release kinetics of the Vv extract from the tested materials, several mathematical models were applied, among which the Weibull and Makoid-Banakar models showed the most promising performance. The choice of the Weibull model was guided by its consistent statistical superiority and its capacity to provide mechanistically meaningful parameters across all formulations.

The Weibull model demonstrated excellent correlation with the experimental data, as evidenced by high determination coefficients (R² values ranging from 0.976 for Gu/Ge/LB/Vv to 0.996 for Gu/Ge/LBSc/Vv) and low reduced chisquared values (between 0.059 and 0.279). These results indicate not only strong data fitting, but also consistency across different material compositions and release profiles. In addition, the Weibull model offered a shape parameter (d) that remained below 1 in all cases, suggesting a Fickian diffusion-controlled release mechanism, which aligns with the expected transport behavior of the tested systems.

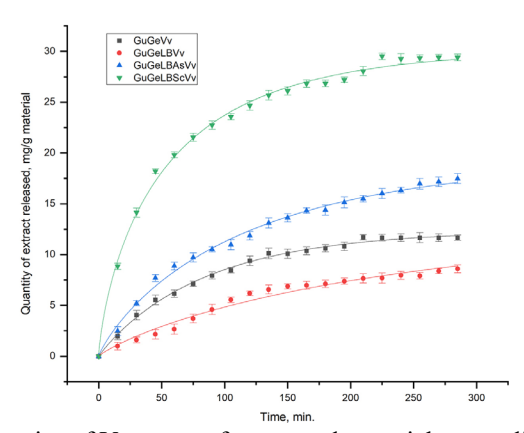


Figure 9: Release kinetics of Vv extract from tested materials according to Weibull model

Table 4
Kinetic parameters of the models applied to the experimental data regarding the release of Vv extract from the obtained materials

-	Gu/Ge/Vv	Gu/Ge/LB/Vv	Gu/Ge/LBAs/Vv	Gu/Ge/LBSc/Vv
Weibull				
\overline{A}	12.391 ± 0.282	13.076 ± 4.523	19.435 ± 1.037	30.297 ± 0.570
x_c	$-7.019 \times 10^{-9} \pm 0.588$	$-6.347 \times 10^{-9} \pm 0.342$	$-3.901 \times 10^{-10} \pm 0.059$	$-4.280 \times 10^{-16} \pm 6.083 \times 10^{-5}$
d	0.953 ± 0.048	0.862 ± 0.149	0.853 ± 0.056	0.746 ± 0.038
k	$0.012 \pm 6.340 \times 10^{-4}$	0.005 ± 0.003	0.009 ± 0.001	$0.018 \pm 9.912 \times 10^{-4}$
red - χ^2	0.059	0.206	0.155	0.279
\mathbb{R}^2	0.995	0.976	0.994	0.996
Korsmeyer-Peppas				

k	1.042 ± 0.157	0.284 ± 0.067	1.122 ± 0.116	5.319 ± 0.514	
n	0.442 ± 0.028	0.613 ± 0.045	0.491 ± 0.019	0.312 ± 0.018	
$red-\chi^2$	0.393	0.309	0.324	1.454	
\mathbb{R}^2	0.969	0.960	0.987	0.977	
		Higuchi			
k	0.774 ± 0.012	0.510 ± 0.012	1.072 ± 0.010	2.018 ± 0.053	
red-χ²	0.455	0.415	0.310	8.055	
\mathbb{R}^2	0.962	0.943	0.987	0.865	
		Makoid-Bana	kar		
k	0.272 ± 0.041	0.025 ± 0.010	0.548 ± 0.101	2.626 ± 0.312	
а	$0.003 \pm 2.785 \times 10^{-4}$	$0.0043 \pm 6.4551 \times 10^{-4}$	$0.001 \pm 3.322 \times 10^{-4}$	$0.002 \pm 2.420 \times 10^{-4}$	
n	0.806 ± 0.039	1.2424 ± 0.0982	0.684 ± 0.046	0.510 ± 0.031	
red-χ²	0.052	0.077	0.148	0.375	
\mathbb{R}^2	0.996	0.990	0.994	0.994	
Gompertz					
а	11.644 ± 0.216	8.290 ± 0.136	17.010 ± 0.531	28.155 ± 0.572	
b	2.226 ± 0.189	3.086 ± 0.221	2.069 ± 0.200	1.887 ± 0.243	
С	0.020 ± 0.001	0.018 ± 0.001	0.015 ± 0.001	0.0269 ± 0.0033	
red-χ²	0.225	0.060	0.766	2.733	
\mathbb{R}^2	0.983	0.992	0.972	0.959	
Hixson-Crowell					
k	$8.741 \times 10^{-4} \pm 5.074 \times 10^{-5}$	$5.766 \times 10^{-4} \pm 2.370 \times 10^{-5}$	$0.001 \pm 6.129 \times 10^{-5}$	$0.003 \pm 1.850 \times 10^{-4}$	
red-χ²	5.051	1.167	6.856	48.802	
\mathbb{R}^2	0.583	0.841	0.722	0.186	

The Makoid–Banakar model also produced statistically strong fits, with R^2 values comparable to those of the Weibull model. For instance, it achieved R^2 values of 0.996 for Gu/Ge/Vv and 0.994 for Gu/Ge/LBAs/Vv. However, its performance was less uniform when evaluating the red- χ^2 values, which ranged more widely, from 0.052 to 0.375. In the case of Gu/Ge/LBSc/Vv, the sample exhibiting the most rapid and extensive release, the Makoid-Banakar model yielded a noticeably higher red- χ^2 value (0.375) compared to the Weibull model (0.279), indicating a comparatively less accurate fit under these conditions.

While the Makoid-Banakar model accounts for both zero-order and first-order contributions to drug release and includes a flexible power term (n), it is primarily empirical and provides limited mechanistic insight. In contrast, the Weibull model not only achieved better overall statistical performance, but also allowed interpretation of the underlying release mechanisms through its kinetic parameters. For example, the scale parameter A from the Weibull equation accurately reflected the maximum amount of extract released (ranging from 12.391 ± 0.282 mg/g for Gu/Ge/Vv to 30.297 ± 0.570 mg/g for Gu/Ge/LBSc/Vv), while the diffusion-driven nature of the release was reflected by shape parameter values consistently below unity.

Based on this combination of strong statistical indicators, reproducibility across formulations, and meaningful mechanistic interpretation, the Weibull model was chosen as the most suitable approach for describing and comparing the release of the Vv extract from the tested materials. Although the Makoid-Banakar model remains a valuable descriptive tool, particularly for systems with mixed release mechanisms, the Weibull model provided the most reliable and interpretable framework for the current study.

Antioxidant activity

The antioxidant activity of the guar/gelatinbased materials (Fig. 10) shows a clear dependence both composition on and physicochemical properties. The incorporation of Vaccinium vitis-idaea extract strongly enhanced radical scavenging capacity, compared to the plain matrix (Gu/Ge), which displayed negligible DPPH inhibition. It is possible that upon adding lignin/lignin ester to the Gu/Ge matrix, its functional groups became less able to neutralize DPPH free radicals, thus hindering its antioxidant efficiency.34 According to Feng et al., the presence of hydrophobic amino acids, aromatic amino acids and sulfur-containing amino acids improves antioxidant activities.³⁵

From Table 2, porosity and water affinity emerge as key drivers of antioxidant efficiency. The Gu/Ge/LBAs/Vv film, with the highest

porosity (0.0143%) and the greatest moisture adsorption (10.24%), achieved some of the most effective radical inhibition, reflecting the contribution of both structural openness and hydrophilic functional groups introduced by lignin aspartate. Similarly, Gu/Ge/LBSc/Vv exhibited moderate porosity (0.0089%), but high density (1.939 g/cm³) and substantial water uptake (8.22%), also supporting efficient solubilization and diffusion of phenolics. By contrast, Gu/Ge/Vv, though enriched in phenolic extract, had lower porosity (0.00167%) and limited water uptake (5.16%), correlating with more modest radical scavenging.

The swelling index values (Fig. 6) confirm this trend. The highest swelling was observed for systems combining Vv extract with lignin esters, suggesting that hydrogen bonding between phenolic groups and ester functionalities promoted water penetration and, consequently, phenolic release. This structural hydration effect was directly reflected in their higher antioxidant activity.

Mechanical testing (Table 3) further supports this interpretation. The addition of the Vv extract decreased tensile strength (from 2.79 MPa in Gu/Ge to 0.39 MPa in Gu/Ge/Vv), while lignin derivatives increased flexibility (elongation at break up to 28.15 mm in Gu/Ge/LB). Notably, Gu/Ge/LBSc/Vv combined low tensile strength (0.37 MPa) with reduced elongation (12.80 mm), creating a more brittle yet porous structure that

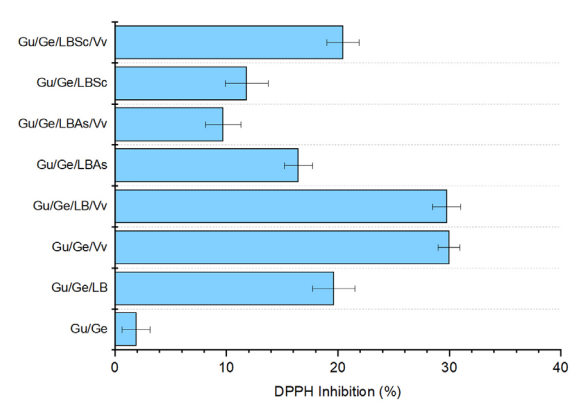


Figure 10: Antioxidant activity of the obtained materials

Anti-inflammatory activity

The anti-inflammatory performance of the guar/gelatin-based films (Fig. 11) follows the same governing principles observed for antioxidant activity: the presence of phenolic

facilitated phenolic release and strong antioxidant action.

SEM micrographs (Fig. 8) revealed that unmodified lignin produced cracked and porous surfaces, while lignin esters combined with Vv generated wrinkled morphologies, improving interfacial compatibility and solvent penetration. This microstructural enhancement explains why lignin ester-Vv systems outperformed both lignin-only and extract-only systems in Figure 10.

The release kinetics of Vv extract (Table 4, Fig. 9) provides a direct quantitative link to antioxidant activity. Gu/Ge/LBSc/Vv released the largest amount of extract (30.3 mg/g) with a high rate constant (k = 0.018), resulting in almost complete (~98%) release. This high release correlated with the strongest radical scavenging among all formulations. Gu/Ge/LBAs/Vv showed moderate release (19.44 mg/g), aligning with its intermediate, but still strong antioxidant response. In contrast, Gu/Ge/LB/Vv provided only ~42% release (13.08 mg/g, k = 0.005), leading to a more modest antioxidant effect despite containing the same amount of extract.

Overall, the highest antioxidant activities were achieved by Gu/Ge/LBSc/Vv and Gu/Ge/LBAs/Vv, owing to their favorable porosity, swelling, and release kinetics. Systems containing only lignin or lignin esters (Gu/Ge/LB, Gu/Ge/LBAs, Gu/Ge/LBSc) displayed much weaker activities, as functional groups of lignin were sterically hindered within the matrix and less available for radical scavenging.

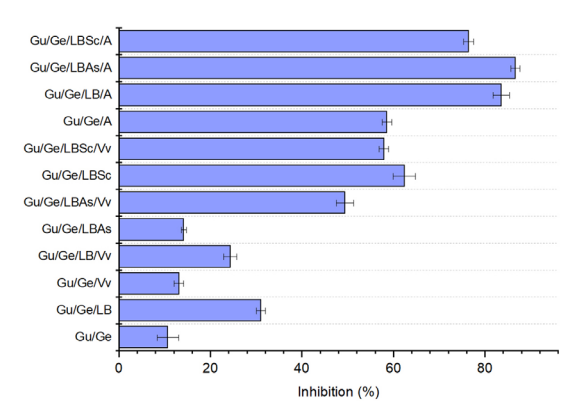


Figure 11: Anti-inflammatory activity of the obtained materials

compounds from the *Vaccinium vitis-idaea* (Vv) extract and the structural modulation introduced by lignin esters.

The plain Gu/Ge matrix exhibited only weak inhibition of protein denaturation, while

incorporation of fillers markedly improved activity. This enhancement can be attributed to the increased hydrophobicity and functional group availability of esterified lignin, which may improve inter- or intramolecular interactions with proteins and thus enhance anti-inflammatory effects.³⁶ The systems containing esterified lignins and Vv extract were the most effective. Specifically, Gu/Ge/LBSc/Vv reached inhibition values above 58%, the highest among all tested samples, correlating with its high extract release (30.30 mg/g) and favorable swelling and porosity properties (porosity 0.0089%, moisture adsorption 8.22%). Similarly, Gu/Ge/LBAs/Vv achieved strong inhibition, exceeding 55%, supported by its highest porosity (0.0143%) and significant release capacity (19.44 mg/g).

By contrast, Gu/Ge/LB/Vv presented lower inhibition, around 45%, in line with its slower and limited extract release (13.08 mg/g, ~42% total release). The materials containing only lignin or lignin esters (without Vv extract) showed the weakest activity (<40% inhibition), underscoring that the polyphenols from Vv were the primary bioactive contributors, while lignin esters acted as structural enhancers.

Thus, the trends in anti-inflammatory action mirror those in antioxidant performance: systems rich in extract and supported by hydrophilic, porous, and swellable matrices (LBSc/Vv, LBAs/Vv) delivered the most effective inhibition of protein denaturation, while compact structures with limited release capacity (LB/Vv, unmodified lignin) lagged behind. An additional advantage of using Vv extract is its broader bioactivity profile,

offering antioxidant effect alongside antiinflammatory action, and its natural origin may improve biocompatibility and reduce potential cytotoxicity compared to synthetic agents.³⁷ Other authors reported that the *Vaccinium vitis-idaea* extract decreased the intracellular ROS level in inflamed adipocytes.³⁸

In vitro biocompatibility of materials (MTS assay)

In vitro biocompatibility of the materials was assessed with an MTS assay after 24 h incubation. All the tested materials presented high cell viability across concentrations of 0.25, 0.5, 0.75 and 1 mg/mL (Fig. 12), with values above 94%. This confirmed the materials' cytocompatibility and potential dermatological use.

The *in vitro* biocompatibility guar/gelatin-based films was assessed on human dermal fibroblasts by MTS after 24 h exposure to extracts corresponding to 0.25, 0.5, 0.75 and 1 mg/mL sample loadings. Across all formulations and doses, cell viability remained ≥94% relative to the control, indicating absence of cytotoxicity and supporting dermatological applicability (Fig. 12). Notably, high viability was preserved even for the compositions that most strongly modulate matrix hydration and release, Gu/Ge/LBAs/Vv (porosity 0.01437%, moisture uptake 10.24%) and Gu/Ge/LBSc/Vv (porosity 0.00887%, moisture uptake 8.22%; density 1.939 g/cm³), demonstrating that increased water accessibility and tighter packing do compromise cytocompatibility.

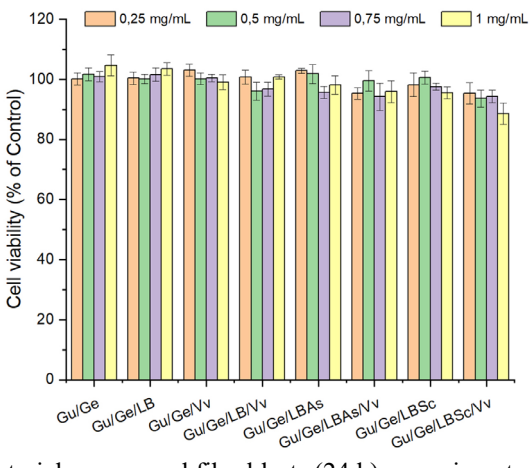


Figure 12: Biocompatibility of materials on normal fibroblasts (24 h); experiments were done in triplicate and treated cell viability was expressed as percentage of control cells' viability

In parallel, the systems with the greatest phenolic delivery (Gu/Ge/LBSc/Vv releasing

30.297 mg/g and Gu/Ge/LBAs/Vv releasing 19.435 mg/g by the Weibull fit) also maintained

≥94% viability, indicating that the diffusional release of Vv polyphenols at the tested levels is well tolerated by HDFs.

By comparison, matrices with more limited release (e.g., Gu/Ge/LB/Vv, A = 13.076 mg/g; ~42% total release under the monitored interval) likewise showed no viability penalty, underscoring that neither the presence of lignin derivatives nor the extract itself introduces acute cytotoxic effects under these conditions.

Taken together, these quantitative comparisons (dose range 0.25–1 mg/mL; minimum recorded viability ≥94%; porosity spanning 0.00062–0.01437%; density 0.710–1.939 g/cm³; Vv release 12.391–30.297 mg/g) attribute the uniformly high biocompatibility to the natural, protein–polysaccharide matrix and to the chemically stabilized incorporation of lignin esters and lingonberry phenolics, whose controlled diffusion does not impair fibroblast metabolic activity.

CONCLUSION

In this study, gelatin-guar materials, incorporating lignin/lignin esters and *Vaccinium vitis-idaea* extract, were prepared and tested as potential skincare products. The physical, mechanical and structural properties of the films were assessed.

The development of these materials opens up opportunities for the utilization of lingonberry extract in various topical formulations. More studies concerning their toxicity and underlying mechanisms of any toxic effects are necessary in order to identify safe use frequency.

present study demonstrated The guar/gelatin matrices enriched with lignin derivatives and Vaccinium vitis-idaea extract represent promising multifunctional biomaterials for skincare applications. Structural analysis confirmed that the incorporation of lignin esters, particularly those derived from aspartic and succinic acid, significantly improved porosity, capacity and hydration, swelling facilitating the release of phenolic compounds. Mechanical testing and morphological observations indicated that, while the addition of bioactive components reduced tensile strength, it also promoted matrix flexibility and heterogeneity, features that support controlled release and surface interaction. Release studies established that Gu/Ge/LBSc/Vv achieved the highest extract delivery (30.30 \pm 0.57 mg/g), followed by Gu/Ge/LBAs/Vv (19.44 ± 1.04 mg/g), with

release kinetics consistent with diffusioncontrolled mechanisms.

These structural and release properties translated into strong biological activities. Antioxidant assays revealed that formulations containing both lignin esters and Vv extract displayed the highest radical scavenging efficiency, while anti-inflammatory evaluation confirmed significant inhibition of protein denaturation (>55% for LBAs/Vv and LBSc/Vv systems). Importantly, all tested materials maintained excellent in vitro biocompatibility, with human dermal fibroblast viability above 94% the tested concentration across range, underscoring their non-cytotoxic character.

Overall, the results highlight a clear correlation between material structure, release behavior and biological performance. By combining natural polysaccharides and proteins with functionalized lignins and phenolic-rich plant extract, this work introduces sustainable and bio-safe matrices with integrated antioxidant, anti-inflammatory and cytocompatible properties. Such multifunctional features recommend these materials as valuable candidates for topical formulations, advanced skincare products and potential biomedical dressings.

REFERENCES

- P. J. Manna, T. Mitra, N. Pramanik, V. Kavitha, A. Gnanamani *et al.*, *Int. J. Biol. Macromol.*, **75**, 437 (2015), https://doi.org/10.1016/j.ijbiomac.2015.01.047
 M. Ahuja, A. Kumar and K. Singh, *Int. J. Biol.*
- Macromol., **51**, 1086 (2012), https://doi.org/https://doi.org/10.1016/j.ijbiomac.2012. 08.023
- ³ X. Pan, Q. Wang, D. Ning, L. Dai, K. Liu *et al.*, *ACS Biomater*. *Sci. Eng.*, **4**, 3397 (2018), https://doi.org/10.1021/acsbiomaterials.8b00657
- ⁴ A. Saarai, V. Kasparkova, T. Sedlacek and P. Saha, J. Mech. Behavior Biomed. Mater., **18**, 152 (2013), https://doi.org/10.1016/j.jmbbm.2012.11.010
- ⁵ J. Boateng, R. Burgos-Amador, O. Okeke and H. Pawar, *Int. J. Biol. Macromol.*, **79**, 63 (2015), https://doi.org/https://doi.org/10.1016/j.ijbiomac.2015. 04.048
- ⁶ I. Spiridon, Cellulose Chem. Technol., **52**, 543 (2018),

https://www.cellulosechemtechnol.ro/pdf/CCT7-8(2018)/p.543-550.pdf

P. Figueiredo, K. Lintinen, J. T. Hirvonen, M. A. Kostiainen and H. A. Santos, *Progress Mater. Sci.*, 93, 233 (2018),

 $\label{eq:https://doi.org/https://doi.org/10.1016/j.pmatsci.2017.1 2.001} \endaligned \footnote{https://doi.org/https://doi.org/10.1016/j.pmatsci.2017.1 2.001}$

- 8 W. Wang, M. Xu, G. Wang and G. Galili, Plant Reprod., 31, 203 (2018),https://doi.org/10.1007/s00497-018-0322-9 G. Resende, G. D. Azevedo, F. Souto and V. ACS 9. 50945 Calado, Omega, https://doi.org/10.1021/acsomega.4c03127 ¹⁰ C. Scarica, R. Suriano, M. Levi, S. Turri and G. Griffini, ACS Sustain. Chem. Eng., 6, 3392 (2018), https://doi.org/10.1021/acssuschemeng.7b03583 ¹¹ D. Urbonaviciene, R. Bobinaite, P. Viskelis, J. Viskelis, A. Petruskevicius et al., Molecules, 28, 12 (2023), https://doi.org/10.3390/molecules28124589 ¹² N. Anghel, M. V. Dinu, M. Zaltariov, D. Pamfil and I. Spiridon, Int. J. Biol. Macromol., 181, 30 (2021), https://doi.org/https://doi.org/10.1016/j.ijbiomac.2021. 03.120 ¹³ P. Dróżdż, V. Šėžienė and K. Pyrzynska, *Plant* Foods Human Nutr.. 72. 360 https://doi.org/10.1007/s11130-017-0640-3
- https://doi.org/10.1007/s11130-017-0640-3

 14 I. Apostol, N. Anghel, M. V. Dinu, F. Ziarelli, A. Mija et al., React. Funct. Polym., 190, 105620 (2023), https://doi.org/10.1016/j.reactfunctpolym.2023.105620

 15 S. Aryal, M. K. Baniya, K. Danekhu, P. Kunwar, R. Gurung et al., Plants (Basel), 8, 4 (2019), https://doi.org/10.3390/plants8040096
- V. Sallustio, M. Rossi, J. Marto, T. Coelho, F. Chinnici *et al.*, *Ind. Crop. Prod.*, **218**, 119042 (2024), https://doi.org/https://doi.org/10.1016/j.indcrop.2024.1 19042
- S. Madihalli, S. P. Masti, M. P. Eelager, R. B. Chougale, B. M. Anilkumar *et al.*, *Int. J. Biol. Macromol.*, 303, 140611 (2025), https://doi.org/10.1016/j.ijbiomac.2025.140611
- ¹⁸ N. Anghel, I. Apostol, I. Plaesu, A. Mija, N. Simionescu *et al.*, *Polymers (Basel)*, **17**, 12 (2025), https://doi.org/10.3390/polym17121707
- F. M. S. Alves, A. K. El Zein, A. F. Cobre, R. E. L. Lazo, J. B. Reolon *et al.*, *J. Drug Deliv. Sci. Technol.*,
 99, 105982 (2024), https://doi.org/10.1016/j.jddst.2024.105982
- ²⁰ A. M. Ramalingam, *Cureus*, **15**, e46003 (2023), https://doi.org/10.7759/cureus.46003
- ²¹ C. Altinkaynak, E. Haciosmanoglu, M. Ekremoglu, M. Hacioglu and N. Özdemir, *J. Biosci. Bioeng.*, **135**, 321 (2023),

https://doi.org/10.1016/j.jbiosc.2023.01.004

- J. Xu, H. Li, H. Yang, T. Wang, Y. Chang et al., J. Food Compos. Anal., 130, 106143 (2024), https://doi.org/10.1016/j.jfca.2024.106143
- ²³ D. N. Olennikov, V. V. Chemposov and N. K. Chirikova, *Foods*, **11**, 18 (2022), https://doi.org/10.3390/foods11182801
- ²⁴ P. Hafezisefat, L. Qi and R. C. Brown, *ACS Sustain*. *Chem. Eng.*, **11**, 17053 (2023), https://doi.org/10.1021/acssuschemeng.3c05221
- ²⁵ S. Li, S. Wu, Y. Wang, J. Jiang, Y. Zhang *et al.*, *Ind. Crop. Prod.*, **224**, 120400 (2025), https://doi.org/10.1016/j.indcrop.2024.120400

²⁶ X. Zhao, Y. Zhang, L. Wei, H. Hu, Z. Huang et al., 52382 RSC Adv.,7, (2017),https://doi.org/10.1039/C7RA10482K ²⁷ A. Coroaba, I. Apostol, I. A. Dascalu, A. Bele, N. L. Marangoci et al., Polymers (Basel), 17, 9 (2025), https://doi.org/10.3390/polym17091221 ²⁸ D. Mudgil, S. Barak and B. S. Khatkar, *Int. J. Biol.* Macromol., **50**, 1035 (2012),https://doi.org/10.1016/j.ijbiomac.2012.02.031 ²⁹ M. L. Picchio, Y. G. Linck, G. A. Monti, L. M. Gugliotta, R. J. Minari et al., Food Hydrocoll., 84, 424 (2018), https://doi.org/10.1016/j.foodhyd.2018.06.028 ³⁰ J. Sujja-Areevath, D. L. Munday, P. J. Cox and K. A. Khan, Eur. J. Pharmaceut. Sci., 6, 207 (1998), https://doi.org/10.1016/S0928-0987(97)00072-9 ³¹ K. Zhao, X. Tian, K. Zhang, N. Huang, Y. Wang et al., Int. J. Biol. Macromol., 226, 202 (2023), https://doi.org/10.1016/j.iibiomac.2022.12.027 ³² M. Sayadi, E. Abedi and N. Oliyaei, LWT, 215, (2025),https://doi.org/10.1016/j.lwt.2024.117241 ³³ R. Jafari, M. Zandi and A. Ganjloo, J. Polym. Environ., (2023),31, 1568 https://doi.org/10.1007/s10924-022-02707-8 ³⁴ R. M. Vieira, E. Gauthier, G. Widanagamage, N. McKenzie, K. Dunn et al., Int. J. Biol. Macromol., 313, 144254 (2025),https://doi.org/10.1016/j.ijbiomac.2025.144254 ³⁵ Y. Feng, D. Yuan, C. Cao, B. Kong, F. Sun et al., Hydrocoll., 131, 107756 https://doi.org/10.1016/j.foodhyd.2022.107756 ³⁶ D. Kai, M. J. Tan, P. L. Chee, Y. K. Chua, Y. L. Yap et al., Green Chem., 18, 1175 (2016), https://doi.org/10.1039/C5GC02616D ³⁷ G. Vilkickyte, M. Zilius, V. Petrikaite and L. Plants 19 Raudone, (Basel), 11, https://doi.org/10.3390/plants11192615 ³⁸ K. Kowalska, A. Olejnik, J. Zielińska-Wasielica and M. Olkowicz, J. Funct. Foods, 54, 371 (2019). https://doi.org/10.1016/j.jff.2019.01.040